Heriot-Watt University
Research Gateway

Investigation of an interlaced laser beam scanning method for ultrashort pulse laser micromachining applications

Citation for published version:
Wlodarczyk, KL, Schille, J, Naumann, L, Lopes, A, Bitharas, I, Bidare, P, Dondieu, S, Blair, P, Loeschner, U, Moore, AJ, Maroto-Valer, MM & Hand, DP 2020, 'Investigation of an interlaced laser beam scanning method for ultrashort pulse laser micromachining applications', *Journal of Materials Processing Technology*, vol. 285, 116807. https://doi.org/10.1016/j.jmatprotec.2020.116807

Digital Object Identifier (DOI):
10.1016/j.jmatprotec.2020.116807

Link:
Link to publication record in Heriot-Watt Research Portal

Document Version:
Publisher's PDF, also known as Version of record

Published In:
Journal of Materials Processing Technology

Publisher Rights Statement:
© 2020 The Authors.

General rights
Copyright for the publications made accessible via Heriot-Watt Research Portal is retained by the author(s) and / or other copyright owners and it is a condition of accessing these publications that users recognise and abide by the legal requirements associated with these rights.

Take down policy
Heriot-Watt University has made every reasonable effort to ensure that the content in Heriot-Watt Research Portal complies with UK legislation. If you believe that the public display of this file breaches copyright please contact open.access@hw.ac.uk providing details, and we will remove access to the work immediately and investigate your claim.

Download date: 04. May. 2023

Journal of Materials Processing Tech. 285 (2020) 116807

Contents lists available at ScienceDirect

Journal of Materials Processing Tech.

journal homepage: www.elsevier.com/locate/jmatprotec

Investigation of an interlaced laser beam scanning method for ultrashort pulse laser micromachining applications

Krystian L. Wlodarczyk[a,b,*], Joerg Schille[c], Lucas Naumann[c], Amiel A. Lopes[a], Ioannis Bitharas[a], Prveen Bidare[a], Stephen D. Dondieu[a], Paul Blair[d], Udo Loeschner[c], Andrew J. Moore[a], M. Mercedes Maroto-Valer[b], Duncan P. Hand[a]

[a] Institute of Photonics and Quantum Sciences, School of Engineering and Physical Sciences, Heriot-Watt University, Edinburgh, EH14 4AS, United Kingdom
[b] Research Centre for Carbon Solutions, School of Engineering and Physical Sciences, Heriot-Watt University, Edinburgh, EH14 4AS, United Kingdom
[c] Mittweida University of Applied Sciences, Laserinstitut Hochschule Mittweida, Schillerstrasse 10, D-09648, Mittweida, Germany
[d] PowerPhotonic Ltd., 5a 1 St David's Drive, St David's Business Park, Dalgety Bay, KY11 9PF, United Kingdom

ARTICLE INFO

Associate Editor: A Clare

Keywords:
Interlaced machining
Ultrashort pulse lasers
Glass
Laser micromachining
Laser process characterisation
Process throughput

ABSTRACT

This article investigates picosecond and sub-picosecond laser micromachining of Borofloat®33 glass and provides clear evidence that a simple modification of the laser beam scanning strategy can lead to significant improvement of machining efficiency and hence process throughput. Besides studying the impact of the fundamental laser machining parameters, such as laser fluence, pulse overlap, pulse repetition frequency (PRF), pulse duration and laser spot diameter, on the machined depth, surface roughness and material removal rate (MRR), it also compares the machining results for two different laser beam scanning strategies, called here "sequential" method (SM) and "interlaced" method (IM). By changing the scanning strategy from SM to IM, the MRR can be significantly increased because IM allows high-quality machining of the glass at higher PRF values. The experimental results show that this simple, cost-free modification allows the MRR value to be increased by more than 4 times, i.e. from 0.12 mm^3/s to 0.53 mm^3/s. Moreover, by using a Phantom V2512 high-speed camera, the picosecond laser micromachining process using both SM and IM was filmed. The videos show that SM leads to the accumulation of glass particles within the laser-machined area, whereas in IM the glass material is removed layer by layer which leads to the generation of "cleaner" and deeper areas. The mechanisms associated with these machining improvements are discussed.

1. Introduction

In modern manufacturing, lasers are recognized as versatile tools that enable non-contact machining of different materials, with high accuracy at micron-scale resolution, via remote control and safe operation. All these features mean that laser-based processes are capable of competing with many conventional processes, such as mechanical cutting, drilling, milling, marking, engraving or surface texturing. In reality, however, machining throughput, process quality and overall cost are the key drivers that determine whether the process is cost-effective and can be applied in industry.

Continuous demand of industry to increase throughput of micromachining processes has encouraged many researchers and companies to develop high average power industrial pulsed lasers. (Malinowski et al., 2013), for instance, developed > 250 W average power fiber lasers capable of producing adjustable pulses in the range of 500 ps to 500 ns with pulse energies more than 10 mJ. (Saraceno et al., 2019), in turn, recently published a review paper in which he describes the progress in the development of high average power ultrafast thin-disk lasers. Nowadays, these lasers can provide average powers at a kW level, producing femtosecond and/or picosecond pulses with energies exceeding 1 mJ.

Modern industrial high average power lasers can produce nanosecond, picosecond and femtosecond pulses with a very high pulse repetition frequency (PRF), even in the MHz range, with pulse energies high enough to machine different materials. This suggests that such lasers should provide efficient machining at very high speeds. Unfortunately, laser machining with a very high PRF does not always lead to higher process throughput because laser-induced heat in a workpiece often causes its overheating, uncontrolled melting,

* Corresponding author at: Institute of Photonics and Quantum Sciences, School of Engineering and Physical Sciences, Heriot-Watt University, Edinburgh, EH14 4AS, United Kingdom.
E-mail address: K.L.Wlodarczyk@hw.ac.uk (K.L. Wlodarczyk).

https://doi.org/10.1016/j.jmatprotec.2020.116807
Received 8 April 2020; Received in revised form 29 May 2020; Accepted 15 June 2020
Available online 18 June 2020
0924-0136/ © 2020 The Authors. Published by Elsevier B.V. This is an open access article under the CC BY license (http://creativecommons.org/licenses/BY/4.0/).

oxidation, bending or even cracking. Moreover, this heat can also lead to the generation of plasma and laser beam shielding that have a detrimental effect on the process speed and machining quality, as observed by (Neuenschwander et al., 2014) during ultrashort pulse laser micromachining of copper and steel. To avoid all these unwanted side effects, laser machining parameters, such as wavelength, pulse duration, fluence, PRF, pulse overlap and scan speed have to be carefully selected for a given workpiece. The best demonstration of this are the experiments described by (Schille et al., 2015) who searched for optimum machining parameters for copper and steel using four different ultrashort pulsed lasers.

To achieve high machining throughput and quality with a high average power laser, the laser machining system has to be equipped with a high-speed laser beam scanning unit, e.g. a modern galvanometer scanner or polygon scanner, to reduce the pulse-to-pulse overlap and prevent the generation of excessive local heat in the workpiece at very high PRFs. Typical galvanometer scanners can move the focused beam with a speed of up 15 m/s across the workpiece (Penning et al., 2016), whereas polygon scanners can provide speeds in the range of 10–300 m/s (Exner et al., 2012). Several researchers have demonstrated high-throughput laser machining using these devices. (Loeschner et al., 2015), for instance, used an in-house developed polygon scanner with a 100 W picosecond laser for machining stainless steel, and achieved a material removal rate (MRR) of 5.4 mm^3/min at PRF = 20 MHz. Only a year later, (Schille et al., 2016) combined a polygon scanner with a galvanometer scan unit, used this setup with a 270 W picosecond laser for machining stainless steel, and achieved the MRR value of 15.3 mm^3/min. In addition to that, they also machined two other metals and Al_2O_3 ceramic and obtained the following MRR values: 27.8 mm^3/min for aluminum, 21.4 mm^3/min for copper and 129.1 mm^3/min for the ceramic.

Another way to increase machining throughput is to split the output laser beam into an array of less powerful beamlets, as demonstrated for instance by (Bruening et al., 2020). This method enables processing of multiple areas on one workpiece or even several workpieces simultaneously. The laser beam splitting can be realized by using beam splitting cubes, prisms, microlens arrays or diffractive optical elements (DOE), such as periodic diffraction gratings or multi-level phase plates (Hofmann et al., 2020). Liquid crystal based spatial light modulators (LC-SLM) can also be used, as demonstrated for instance by (Wlodarczyk et al., 2014). These devices, sometimes called programmable DOEs, enable dynamic modification of the number of beamlets and their spatial distribution on the fly. Recently, (Gillner et al., 2019) has also shown that multiple laser beams for high speed machining can be generated and efficiently controlled by combining an acousto-optic and phase modulating beam steering system together with a diffractive optical beam splitter.

This article investigates micromachining of borosilicate (Borofloat®33) glass using ultrafast, picosecond and sub-picosecond pulsed lasers. In general, such lasers are highly suitable tools for processing glass materials. The very short interaction time of individual laser pulses with the workpiece leads to the generation of a very small heat-affected zone (HAZ) in the surroundings of the machined area, providing “crack-free” removal of glass with very high precision and sub-micron spatial resolution. Previous publications have shown that a picosecond pulsed laser can successfully be used for cutting and microdrilling thin flex glass sheets (Wlodarczyk et al., 2016) and also for drilling and micro-milling millimeter-thick borosilicate glass plates (Wlodarczyk et al., 2019a, 2018). The last two publications have also shown that the same laser is capable of welding two glass plates together, and can be used for rapid prototyping microfluidic devices for various applications in the field of carbon storage and petroleum engineering research. In combination with a CO_2 laser, ultrafast lasers can also be used for the manufacturing of bespoke optics and micro-optics. (Schwarz and Hellmann, 2017), for instance, used a femtosecond pulsed laser to generate a cylindrical shape on the surface of fused silica, and then a 60 W CO_2 laser to obtain optically-smooth surface finish. More recently, the same researchers have shown that this two-step laser process can also be used for the fabrication of high-quality axicons (Schwarz et al., 2018) and axicon arrays (Schwarz et al., 2020).

The purpose of the work described in this article is to examine the impact of the laser beam scanning strategy on process throughput and machining quality for Borofloat®33 glass. Besides studying the impact of the fundamental laser machining parameters, such as laser fluence, pulse overlap and PRF, on the machined depth, surface roughness and MRR, two different laser beam scanning strategies, called here "sequential” method (SM) and “interlaced” method (IM), are investigated. As reported by (Neuenschwander et al., 2016), IM can significantly improve surface finish of ultrashort pulse laser machined metals. The machining results presented in this article were generated using two ultrashort pulse lasers (Trumpf TruMicro 5 × 50 and Edgewave FX 200) that operated at the 1030 nm wavelength. This work, however, also refers to another paper (Wlodarczyk et al., 2019b) that describes the picosecond laser micromachining of Borofloat®33 glass using a shorter laser wavelength (λ = 515 nm). The article also presents videos recorded by a Phantom V2512 high-speed camera that show the laser beam interaction with glass during the picosecond laser micromachining using both SM and IM. Thanks to these videos, the mechanisms that lead to the machining improvements obtained using IM can be explained.

2. Equipment and methodology

2.1. Materials

All laser machining experiments described in this article were performed using 1.1 mm thick borosilicate glass plates (Borofloat®33, SCHOTT Technical Glass Solutions GmbH), supplied by Newcastle Optical Engineering Ltd. (UK). The key characteristics of Borofloat®33 are: outstanding thermal resistance, high optical transparency and chemical durability, and excellent mechanical strength.

2.2. Laser processing workstations

Two ultrashort pulse laser machining systems were used to perform a comparative study between SM and IM. The first laser machining system located at Heriot-Watt University in Edinburgh (UK) uses a 50 W Trumpf picosecond laser (TruMicro 5 × 50), whereas the other laser system located at the University of Applied Sciences in Mittweida (Germany) uses a 100 W sub-picosecond laser (Edgewave FX 200). The Trumpf laser produces 6 ps pulses, measured as Full-Width-Half-Maximum (FWHM), at λ = 1030 nm. According to the manufacturer, the maximum pulse energy (E_{PMAX}) is 125 μJ and the maximum pulse repetition frequency (PRF_{MAX}) is 400 kHz. In this laser system, the laser beam diameter in the focus is approximately 41 μm, obtained by using a 160 mm focal length F-theta lens mounted to a HSR 10 galvanometer scanner (Trumpf). The laser spot diameter was measured at $1/e^2$ of its maximum intensity, using a Beam-Map 2 scanning slit beam profiler (DataRay). The Edgewave laser, meanwhile, produces 600 fs pulses at λ = 1030 nm with E_{PMAX} = 50 μJ for the PRF values up to 2 MHz. The laser can also produce sub-picosecond pulses with a higher PRF (up to 50 MHz) but at the cost of reduced pulse energy. In this laser system, the laser beam is focused to a 30 μm diameter spot, as measured using a MicroSpotMonitor camera-based focus analysis system (Primes GmbH), using a 167 mm focal length, fused silica, telecentric F-Theta lens. The lens is mounted to a high-speed galvanometer scanning unit (intelliSCAN 30, ScanLab GmbH) which was equipped with SiC-substrate mirrors. In this configuration, the galvanometer scanner enables the translation of the laser beam across the workpiece at speeds up to 11.8 m/s (when only one axis is involved) and 16.8 m/s (during diagonal translation when both axes are involved).

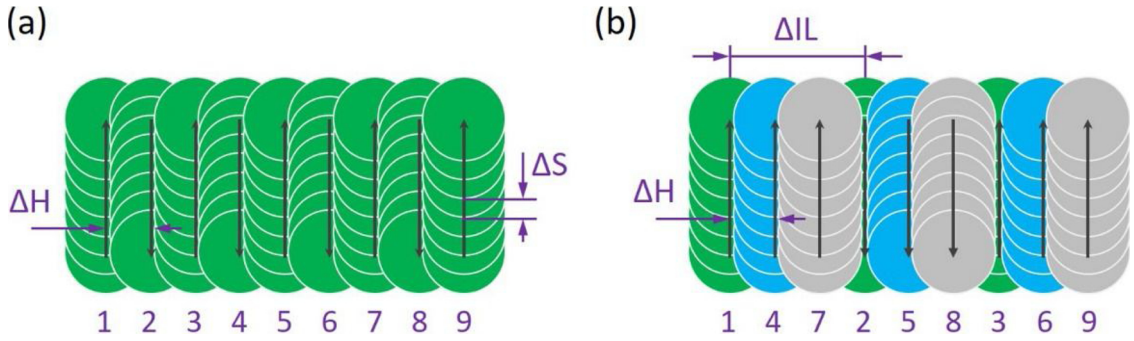

Fig. 1. Illustration of bi-directional: (a) sequential and (b) interlaced laser beam scanning method. Symbols: ΔH – hatch distance, ΔS – pulse-to-pulse distance along the linear movement of the laser beam, and ΔIL – interlacing distance.

2.3. Laser beam scanning methods

Fig. 1 shows two laser beam scanning methods that were used in the experiments described in this paper. The first scanning method, named here "sequential" method (SM), is very well-known and commonly used for laser micromachining. In SM, the laser beam is translated following the pattern shown in Fig. 1(a). The arrows indicate the direction of the laser beam movement, whereas the numbers indicate the scanning sequence.

The second scanning method, named here "interlaced" method (IM), is less known and most likely not currently available as a standard hatch pattern in any commercial laser beam scanning software. In IM, as illustrated in Fig. 1(b), some scanning lines are deliberately omitted at regular intervals during the first pass in order to be filled later in subsequent laser beam passes. In subsequent passes, the laser beam starts scanning at an offset equal to the hatch distance (ΔH) in relation to the previous pass, omitting an identical number of scanning lines as before. The interlacing is repeated until all the missing lines are filled in. The number of repetitions is defined as a ratio of ΔIL to ΔH, where ΔIL is an interlacing distance. More information about IM can be found in (Wlodarczyk et al., 2019b).

2.4. Experiments

The experiments relied on laser machining of small areas, typically 2 mm × 2 mm, on the upper surface of Borofloat®33 glass plates, as shown in Fig. 2. Each "test area" was machined using a different set of laser processing parameters, applying one of the two laser beam scanning methods (either SM or IM). The laser machining variables were peak laser fluence (F), pulse repetition frequency (PRF), and pulse overlap (O). For simplicity, the pulse overlap along the laser beam scan direction (O_S) was the same as the pulse overlap in the hatch direction (O_H). These two pulse overlaps were calculated as follows:

$$O_S = [1 - (\Delta S / 2\omega)] \times 100\ \%, \quad (1)$$

$$O_H = [1 - (\Delta H / 2\omega)] \times 100\ \%, \quad (2)$$

where 2ω is the laser spot diameter. All laser machining parameters used in the experiments are listed in the Supplementary Materials (see Tables S1-S12).

Before laser machining, the borosilicate glass plates were washed in isopropanol and wiped using soft lens tissues in order to remove dust, contamination and fingerprints. The test areas were produced with the laser beam focused on the upper surface of the glass. The glass samples were suspended in a special holder so that the machining area had a clear aperture underneath.

2.5. Cleaning and analysis of the laser machined areas

Fig. 2 shows that following the laser process the glass plates were contaminated by small glass particles (white powder). These particles were removed by placing the glass plates inside a beaker filled with methanol. The beaker was placed inside an ultrasonic cleaner for a few minutes. Following the ultrasonic bath treatment, the laser-machined areas were inspected using a Leica optical microscope (DM6000 M), and measured using an Alicona 3D surface profilometer (InfiniteFocus). Machined area depths were measured using a ×5 zoom objective, whereas surface roughness was measured using ×10 zoom objective. The field of view of the second objective was 1.43 mm by 1.08 mm. For the glass samples machined using the Edgewave laser system, the test areas were measured using a Keyence 3D laser scanning microscope (VK-X250 K).

The picosecond laser micromachining of glass using both SM and IM was filmed using a Phantom V2512 high speed monochrome camera. The captured videos allowed direct observation of the differences between the SM and IM machining processes. The SM and IM processes were filmed at 10,000 frames per second (fps) and a resolution of 768 × 768 pixels. The camera was placed at an angle of approximately 80 degrees with respect to the glass workpiece surface. During the video

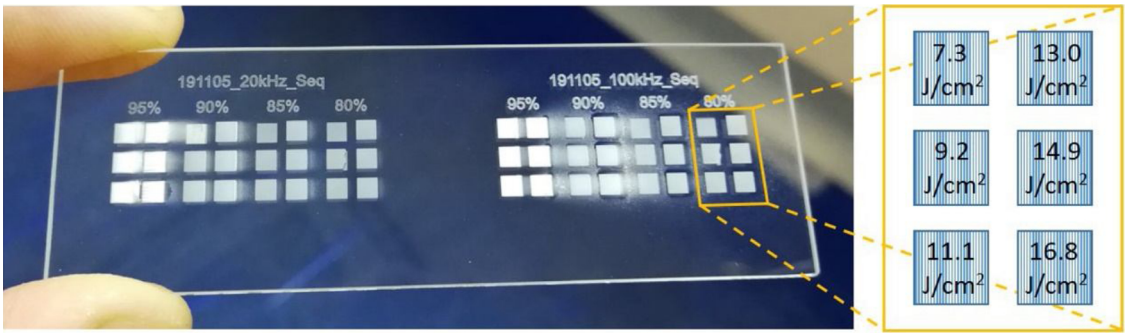

Fig. 2. Photograph of Borofloat®33 glass plate just after picosecond laser machining using SM. The illustration on right shows the peak laser fluence values used for machining squares.

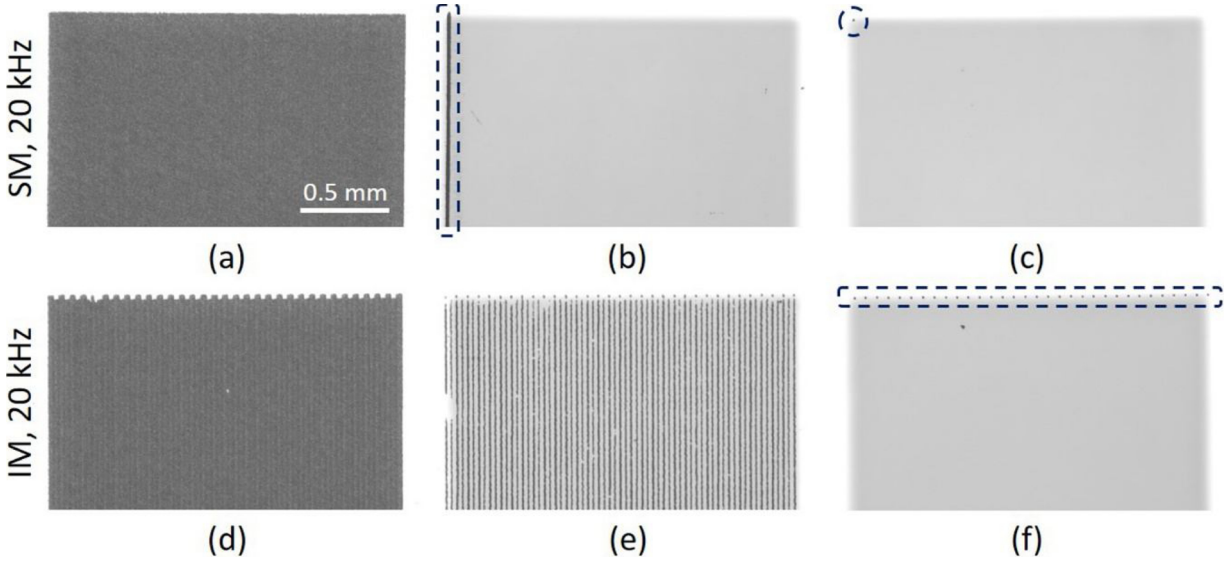

Fig. 3. Leica microscope images of the rear surface of Borofloat®33 glass machined using (1st row) SM and PRF = 20 kHz and (2nd row) IM with ΔIL = 32 μm and PRF = 20 kHz. Laser fluence and pulse overlap were as follows: (a) 7.3 J/cm^2, 85 %, (b) 7.3 J/cm^2, 95 %, (c) 9.2 J/cm^2, 95 %, (d) 7.3 J/cm^2, 85 %; (e) 11.1 J/cm^2, 85 %, (f) 9.2 J/cm^2, 95 %. Dashed circle and boxes indicate different "minor" damages.

recording, the region of interest was illuminated by using a high brightness light-emitting diode.

3. Results

3.1. Machining of glass using 6 ps laser pulses

Using the Trumpf laser machining system, each set of twenty four test areas (see Fig. 2) was produced by applying one of the four pulse repetition frequency values (PRF = 20 kHz, 100 kHz, 200 kHz or 400 kHz). Four different pulse overlaps (O = 80 %, 85 %, 90 % or 95 %) were used, each for six squares, while each square of the six was produced using a different value of peak laser fluence (F = 7.3, 9.2, 11.1, 13.0, 14.9 or 16.8 J/cm^2). The laser machining was performed using SM, and then repeated for a new glass plate using IM.

3.1.1. Optical microscope inspection of the laser-machined areas

During this inspection, it was observed that the laser beam always caused damage to the rear surface of the glass, despite focusing the laser beam on the upper surface of the material. The damage was either within the entire area, as shown in Fig. 3(a), (d) and (e), along one or two edges, as shown in Fig. 3 (b) and (f), or only in one corner, as can be seen in Fig. 3 (c). In the case when the entire rear surface was damaged (see Fig. 3 (a) and (d)), laser ablation did not occur on the upper surface. In the other cases, laser ablation occurred on both surfaces.

The results of the optical inspection for the laser-machined glass samples were summarized in Table 1 for SM and Table 2 for IM using ΔIL = 32 μm. The reason why the ΔIL of 32 μm was selected is explained in Section 3.1.3.

Table 1
Results of the inspection of the rear surface of the glass plates machined using SM. Symbols: WA – severe damage within the entire area, Line – local damage along one edge, Dot – minor damage in one corner. Blue areas highlight areas with glass particles firmly attached to the upper glass surface.

F [J/cm^2]	20 kHz				100 kHz			
	80%	85%	90%	95%	80%	85%	90%	95%
7.3	WA	WA	WA	Line	WA	WA	WA	Line
9.2	WA	Line	Line	Dot	WA	WA	Dot	Dot
11.1	Line	Line	Dot	Dot	Line	Line	Dot	Dot
13.0	Line	Line	Dot	Dot	Line	Line	Dot	Dot
14.9	Line	Line	Dot	Dot	Line	Line	Dot	Dot
16.8	Line	Dot	Dot	Dot	Line	Dot	Dot	Dot

With a peak laser fluence (F) slightly above 7 J/cm^2, machining occurred only at the rear surface. The exceptions were two areas produced using SM, O = 95 %, and PRF = 20 kHz and 100 kHz (see Table 1). Although both areas had minor damages on the rear surface, seen as a line in Fig. 3(b), the area machined using PRF = 100 kHz had also a substantial amount of white powder on the upper surface. This powder contained small glass particles; some of which were so firmly attached to the machined area that they could not be removed using the ultrasonic cleaner. A similar issue was observed in most areas machined using SM and O = 95 %. These areas are highlighted in blue in Table 1. The white powder was also noted within the areas machined using SM with PRF = 200 kHz and 400 kHz, even in the areas produced with O < 95 %.

In the case of IM, the rear surface of the glass had either severe damage within the entire machined area or minor damage only along two opposite edges. For low values of laser fluence, surface damage was within the entire area, as shown in Fig. 3(d), and laser ablation did not occur on the upper surface of the glass. For higher values of laser fluence and O ≤ 85 %, the laser beam machined the upper surface, but also periodically damaged the rear surface of the glass (see Fig. 3(e) as an example). In the areas highlighted in green in Table 2, damage on the rear surface had a form of an array of dots, as shown in Fig. 3(f). The dots were on two opposite edges. The other edge is not seen in Fig. 3(f).

3.1.2. Sequential machining (SM)

Only the areas highlighted in yellow and green in Table 1 were measured using the Alicona surface profilometer in order to determine their average depth and surface roughness. In these areas, the rear surface of the glass had minor damage, only either along one edge or in one corner. The presence of white powder in the areas generated with O = 95 % and PRF > 100 kHz led to misleading measurements, i.e. underestimated depths and overestimated surface roughness, therefore these results were not analyzed any further.

The measurement results for two PRF values and four pulse overlaps are shown in Fig. 4. Using SM, PRF = 20 kHz and O = 95 %, see Fig. 4(a), it was possible to remove approximately a 70 μm deep layer of glass in a single laser pass. In general, the machined depth (D) was dependent on the peak laser fluence (F) and pulse overlap (O), but was less dependent on the PRF value. Regarding the surface roughness, the

Table 2
Results of the inspection of the rear surface of the glass plates machined using IM and ΔIL = 32 µm. Symbols: WA – severe damage within the entire area, Dots – dotted damage along two opposite edges.

F	20 kHz			100 kHz			200 kHz			400 kHz		
[J/cm^2]	≤85%	90%	95%	≤85%	90%	95%	≤85%	90%	95%	≤85%	90%	95%
7.3	WA	WA	WA	WA	WA	WA	WA	WA	WA	WA	WA	WA
9.2	WA	WA	Dots	WA	WA	Dots	WA	WA	Dots	WA	WA	Dots
11.1	WA	WA	Dots	WA	Dots	Dots	WA	Dots	Dots	WA	Dots	Dots
13.0	WA	Dots	Dots	WA	Dots	Dots	WA	Dots	Dots	WA	Dots	Dots
14.9	WA	Dots	Dots	WA	Dots	Dots	WA	Dots	Dots	WA	Dots	Dots
16.8	WA	Dots	Dots	WA	Dots	Dots	WA	Dots	Dots	WA	Dots	Dots

root-mean-square (S_q) value of almost all analysed areas was in the range of 1.2–1.6 µm. The exception was the area machined using PRF = 100 kHz, F = 16.8 J/cm^2 and O = 90 %, where the S_q value was 1.8 µm. Here it must be noted that the error bars in Fig. 4(a) and (c) represent the S10z (Ten-point height) values calculated according to the international standard ISO 12781-1:2003.

The material removal rate (MRR) for different combinations of laser machining parameters was also calculated, and these results are shown in Fig. 5. As expected, higher MRR values were obtained with PRF = 100 kHz due to the higher scan speeds used to maintain the same pulse overlap. The highest MRR value of approximately 0.12 mm^3/s was measured for the maximum laser fluence (F = 16.8 J/cm^2) and O = 80 %. A slightly lower MRR was obtained with O = 85 %.

3.1.3. Interlaced machining (IM)

The number of skipped lines in each laser beam pass, which is defined by an interlacing distance (ΔIL), as illustrated in Fig. 1(b), was found to be a key parameter that significantly affects the depth and surface roughness of the areas machined using IM. Evidence of this is shown in Fig. 6, where the test areas were produced using a constant fluence (F = 16.8 J/cm^2), PRF = 100 kHz, and O = 90 % (ΔS = ΔH = 4 µm). The only variable here was the interlacing distance (ΔIL) which was different for each area.

In the case when ΔIL = ΔH, the area was machined in the same way as using SM. For increasing values of ΔIL, as can be seen in Fig. 6, the areas at the bottom start having parallel furrows whose periodicity increases with increasing ΔIL. The furrows become very pronounced for ΔIL ≥ 28 µm and their periodicity corresponds to ΔIL.

The same experiment was also repeated for O = 95 % (ΔS = ΔH = 2 µm) and the results of this experiment are shown in Fig. 7. For ΔIL ≤ 12 µm, the machined areas were covered by glass particles firmly attached to the glass surface, because the machining conditions were the same or very similar to SM. Interestingly, for ΔIL = 12 µm, the rear surface had also slightly skewed parallel furrows whose periodicity was

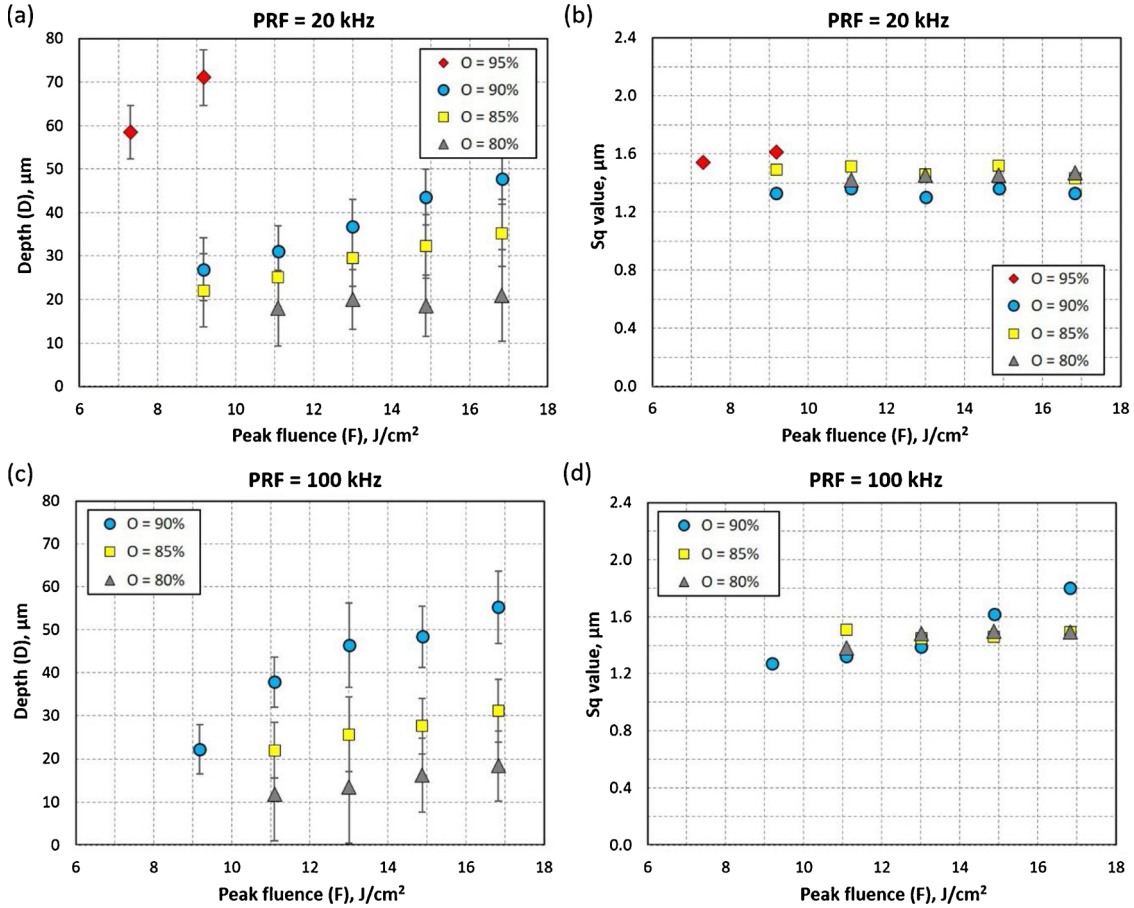

Fig. 4. Depth and Sq value of the areas machined using SM as a function of peak laser fluence. Results were obtained with: (a) and (b) PRF = 20 kHz, (c) and (d) PRF = 100 kHz. Error bars in (a) and (c) show the S10z values calculated according to ISO 12781-1:2003.

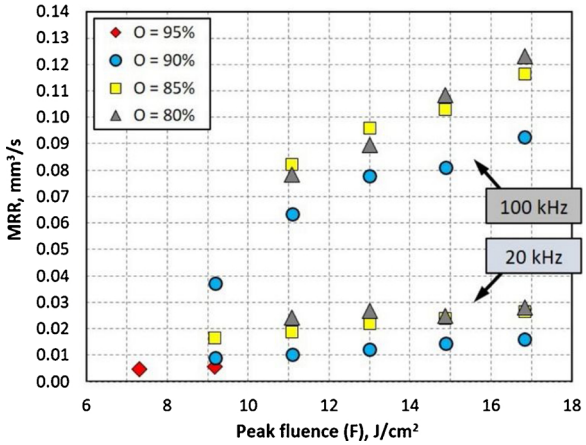

Fig. 5. Material removal rate (MRR) obtained using SM as a function of peak laser fluence. Results are shown for PRF = 20 kHz and 100 kHz.

approximately 85 µm. For the areas machined using ΔIL > 12 µm, the furrows were also present and were similar to those observed in the areas produced with O = 90 %. As before, the periodicity of these furrows corresponded to ΔIL. By comparing Fig. 6 with Fig. 7, it can be noted that the areas machined with the higher pulse overlap seem to be rougher, in particular when ΔIL ≤ 40 µm. To confirm this observation, the mean depth and surface roughness of each machined area was measured using the Alicona profilometer.

As can be seen in Fig. 8, both mean depth and surface roughness depend on the value of pulse overlap and the interlacing distance used for machining. For O = 90 %, the machined depth increases for low values of ΔIL and then stays in the range of 75–100 µm. The surface roughness (S_q value), in turn, oscillates near 2 µm and then increases when ΔIL > 32 µm. For O = 95 %, the influence of ΔIL on the mean depth and S_q value is more pronounced. When ΔIL is between 16 µm and 32 µm, the depth of the machined areas increases from 300 µm to 400 µm. The S_q value for this range of ΔIL is below 4.2 µm. Although the highest depth was obtained using ΔIL = 36 µm, the Sq value of this area was nearly 7 µm. Further increases of ΔIL resulted in less efficient machining, because the machined depth started decreasing rapidly (to the mean value of approximately 100 µm), whereas the Sq value started rapidly increasing.

Following the above experiments, the ΔIL of 32 µm was used to produce more test areas on Borofloat®33 glass using IM because this value seemed to provide the best machining results, i.e. high machined depth and relatively low surface roughness. After the optical inspection of the IM machined areas, as described in Section 3.1.1, only those produced with O = 90 % and 95 % were analyzed using the Alicona surface profilometer.

Mean depths and Sq values of the areas machined with O = 90 % are plotted as a function of peak fluence in Fig. 9(a) and (b), respectively, whereas the values for the areas machined with O = 95 % are plotted in Fig. 9(c) and (d). For both pulse overlap values, the mean depth increases almost linearly with increasing laser fluence, regardless of the PRF used, reaching 90 µm for O = 90 % and PRF = 100 kHz, and 400 µm for O = 95 % and PRF = 100 kHz, as expected, given the results plotted in Fig. 8(a). The surface roughness produced with O = 90

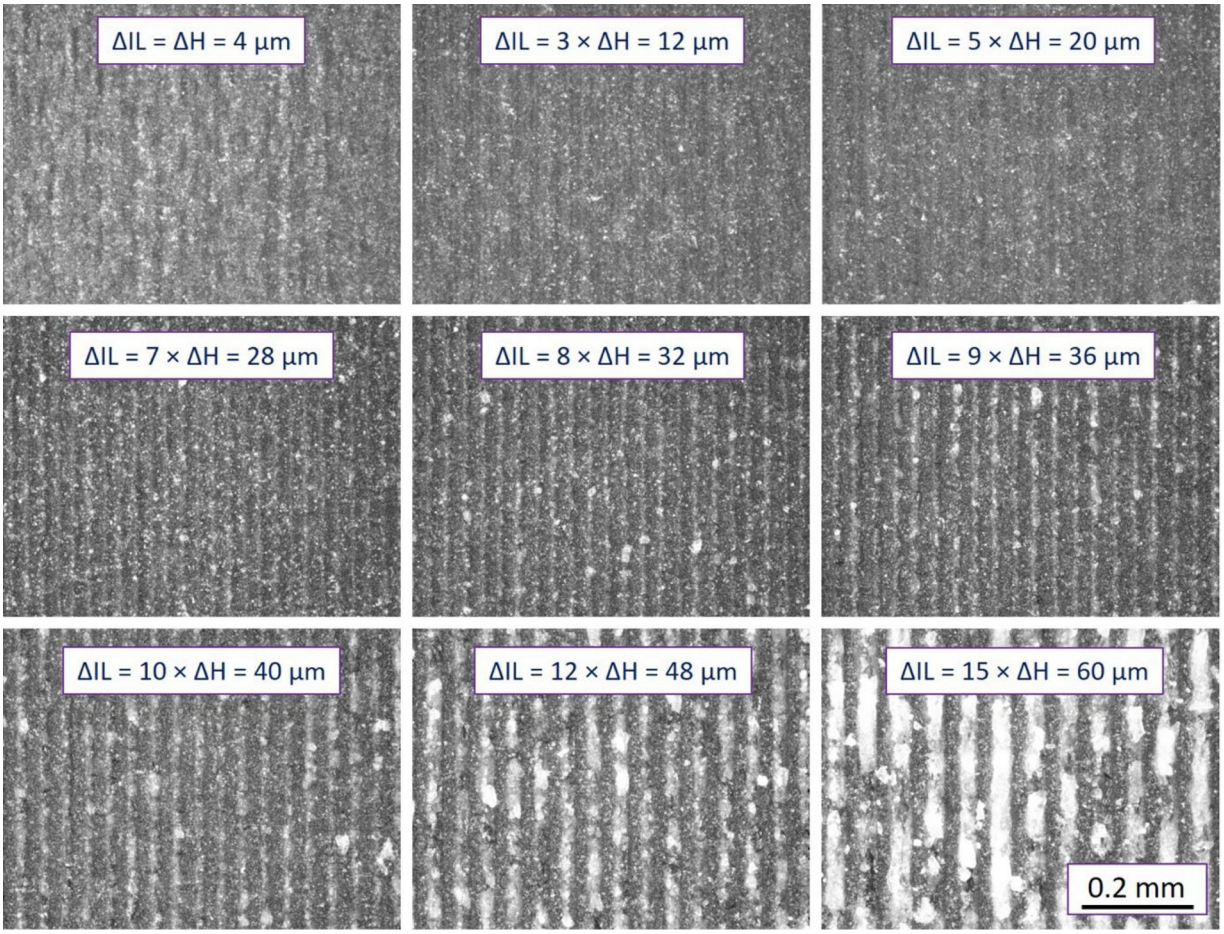

Fig. 6. Top view of the center of the areas machined using different interlacing distances (ΔIL) and F = 16.8 J/cm^2, PRF = 100 kHz, and ΔH = 4 µm. The images were captured using the Alicona surface profilometer.

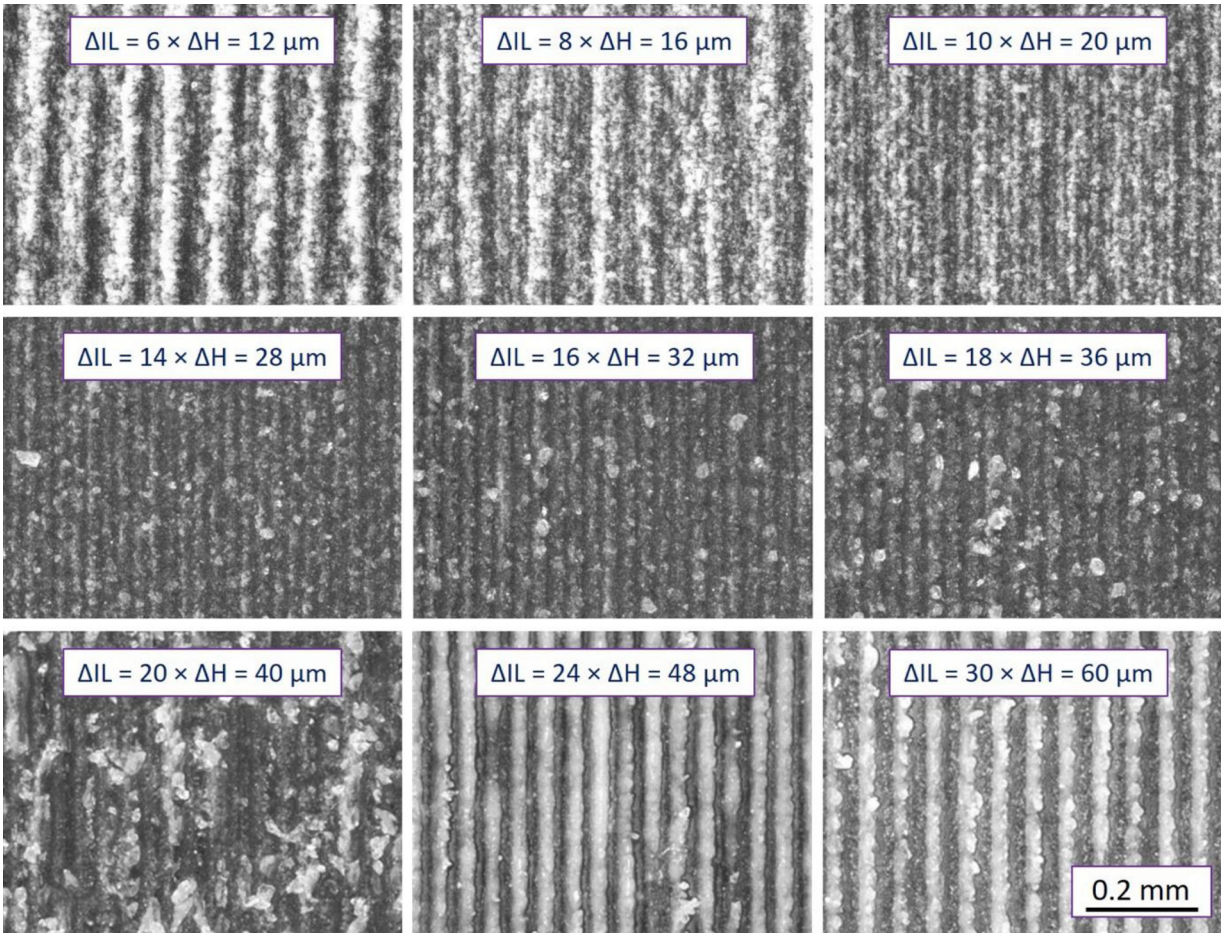

Fig. 7. Top view of the center of the areas machined using different interlacing distances (ΔIL) and F = 16.8 J/cm^2, PRF = 100 kHz, and ΔH = 2 µm. The images were captured using the Alicona surface profilometer.

% was in the range of 1.5–2.5 µm, as shown in Fig. 9(b). Interestingly, the highest S_q values were obtained with PRF = 100 kHz, not with higher PRF values at which theoretically the process could be less stable due to excessive heating and the formation of white powder, as observed for SM. In the case of the areas generated with O = 95 %, the S_q value decreases with increasing laser fluence when PRF ≥ 100 kHz, see Fig. 9(d). For PRF = 20 kHz, the surface roughness was always below 3 µm.

Based on the results shown in Fig. 9, the MRR values were calculated. It is not surprising that the highest MRR values were obtained with PRF = 400 kHz (see Fig. 10). Using F = 16.8 J/cm^2, it was possible to ablate the material as fast as 0.43 mm^3/s (using O = 90 %) and 0.53 mm^3/s (using O = 95 %). These values of MRR are therefore at least 3.5 times higher than those obtained using SM (see Fig. 5) where the PRF was limited to 100 kHz.

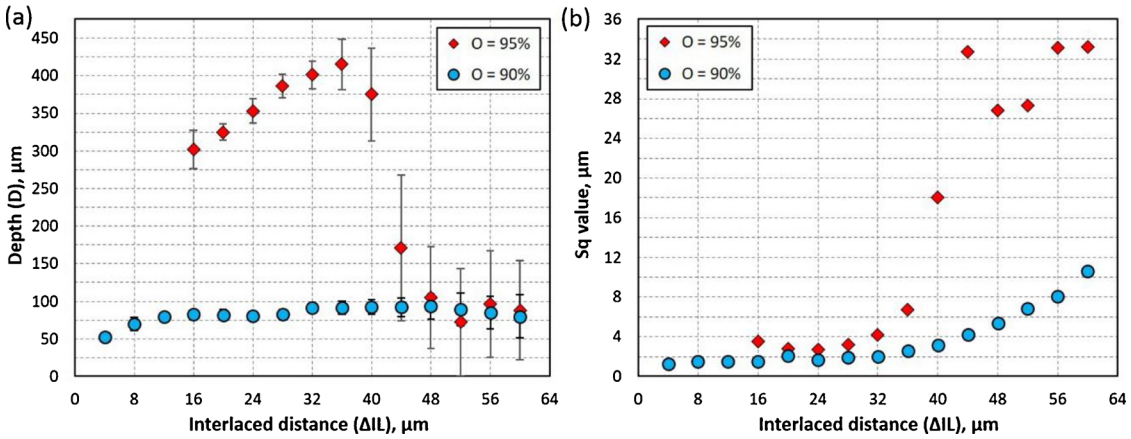

Fig. 8. Influence of the interlaced distance (ΔIL) on the depth and Sq value of the laser machined areas. Results presented for 90 % and 95 % pulse overlap, E_P = 16.8 J/cm^2 and PRF = 100 kHz. Error bars in (a) show the S10z values calculated according to ISO 12781-1:2003.

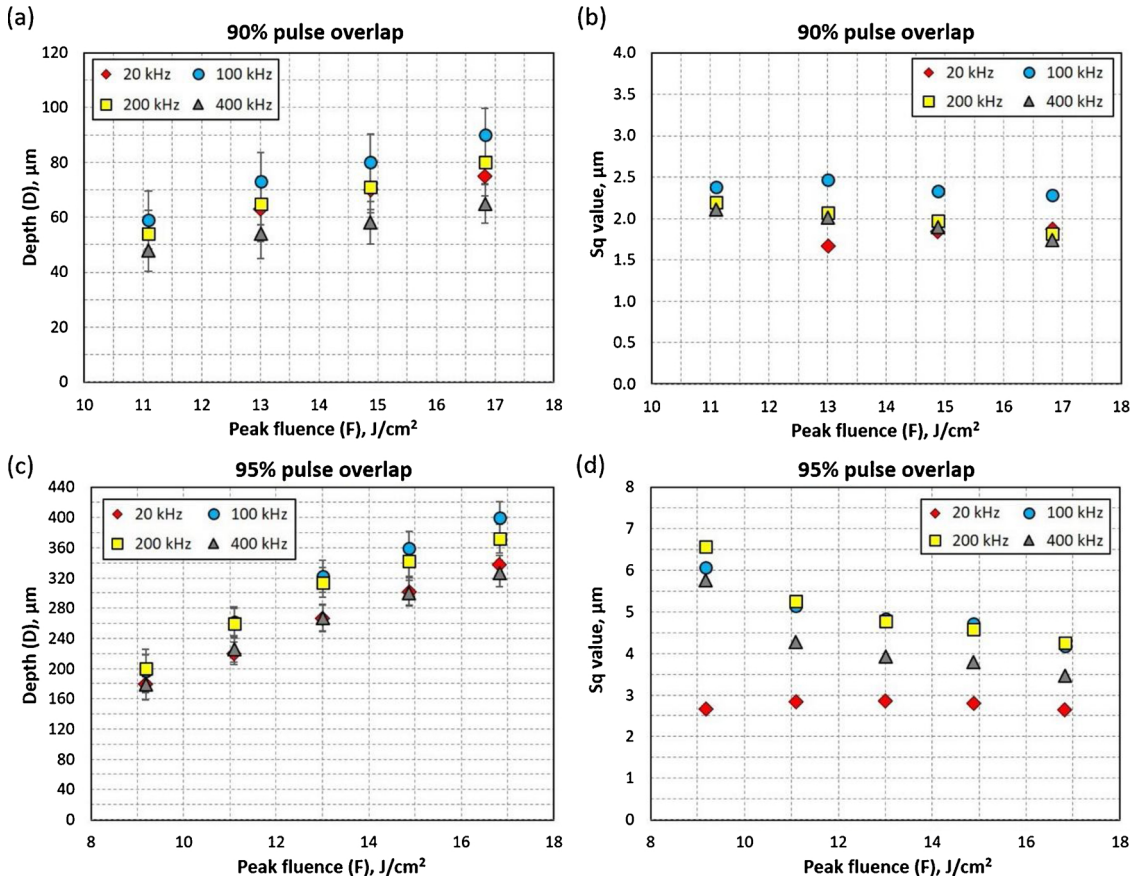

Fig. 9. Depth and Sq value of the areas machined using IM (with ΔIL = 32 µm) as a function of peak laser fluence used. Results were obtained with: (a) and (b) 90 % pulse overlap, (c) and (d) 95 % pulse overlap. Error bars in (a) and (c) show the S10z values calculated according to ISO 12781-1:2003.

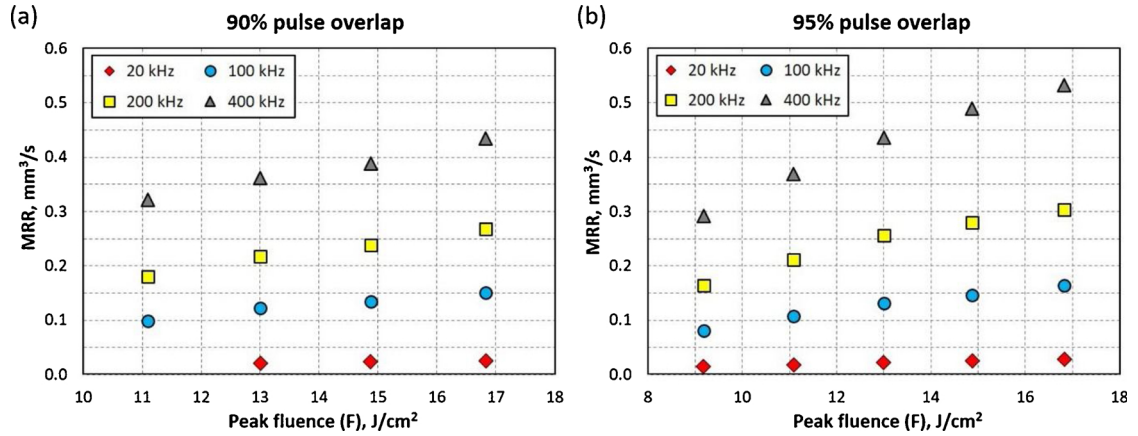

Fig. 10. Material removal rate (MRR) obtained using IM (with ΔIL = 32 µm) as a function of peak fluence. Results presented for: (a) 90 % pulse overlap and (b) 95 % pulse overlap.

3.2. Machining of glass using sub-picosecond laser pulses

Similar test areas were also generated on the surface of Borofloat®33 glass by using the Edgewave laser machining system. The machining was performed for a wider range of PRF values (between 100 kHz and 1.95 MHz). Thanks to the modern high-speed galvo scanning unit, it was possible to machine the glass using the same pulse overlap values as in the experiments performed with the Trumpf laser. The maximum pulse energy used was 45.2 µJ, corresponding to F = 12.8 J/cm^2. The aim of this work was to investigate IM for shorter laser pulse durations and higher pulse repetition rates.

The mean depth of the areas machined using SM and IM are plotted as a function of PRF in Fig. 11(a) and (b), respectively, for a fixed value of laser fluence (F = 10.6 J/cm^2) and different O values. In IM, the interlacing distance (ΔIL) was 18 µm for O = 80 % and 85 % and 15 µm for O = 90 %. The results for the areas generated with O = 95 % are not presented because these areas were heavily covered by white powder (i.e. glass particles). This powder was present within the areas machined using both SM and IM.

For O = 80 % and 85 %, the machined depths obtained using IM are very similar to those produced using SM. The difference, however, is obvious for O = 90 %. In SM, as can be seen in Fig. 11(a), the machined

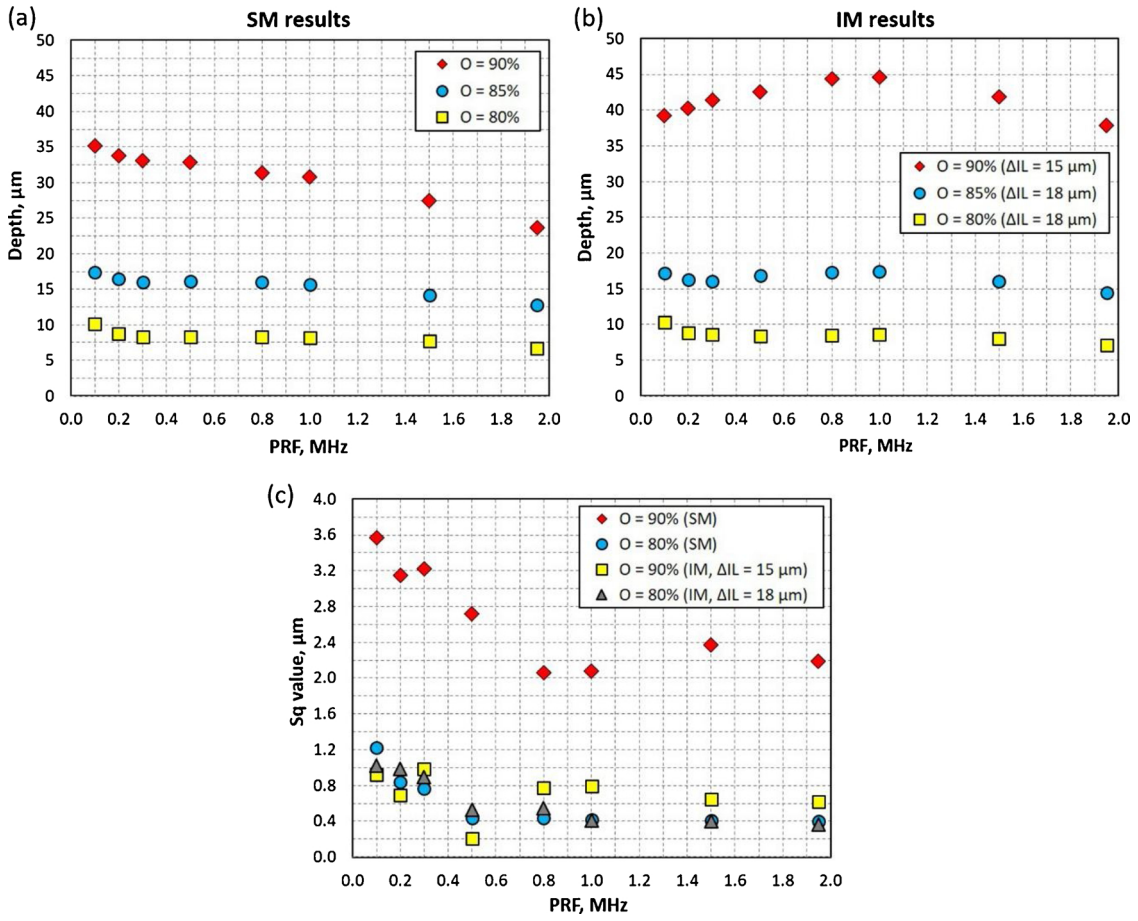

Fig. 11. Influence of PRF on: (a), (b) the depth and (c) the S_q value of the areas machined using the Edgewave laser with F = 10.6 J/cm^2. The depth results are presented for: (a) SM and (b) IM using ΔIL = 15 µm for O = 90 % and ΔIL = 18 µm for O = 80 % and 85 %.

depth decreases with increasing PRF, whereas the machined depth obtained using IM increases, to approximately 45 µm when PRF = 1 MHz, and then decreases when PRF > 1 MHz. For PRF = 1 MHz and O = 90 %, the machined depth obtained using IM is almost 50 % higher than the depth obtained using SM.

The Sq values plotted in Fig. 11(c) show that an increase of PRF typically leads to the generation of areas with a smoother surface. Although the S_q values of the surfaces generated using O = 80 % are very similar for both SM and IM, the differences are significant for O = 90 % (e.g. 2.1 µm vs. 0.8 µm for PRF = 1 MHz).

Fig. 12 shows that MRR increases almost linearly with increasing PRF, in particular when PRF ≤ 1 MHz. For higher PRF values, this linear dependency disappears but MRR still increases. In SM, the highest MRR value of 0.50 mm^3/s was obtained by using O = 85 %, whereas in IM the highest MRR value of 0.66 mm^3/s was obtained with O = 90 %. This corresponds to an increase of MRR by approximately 30 %.

The impact of laser fluence on the machined depth, S_q value and

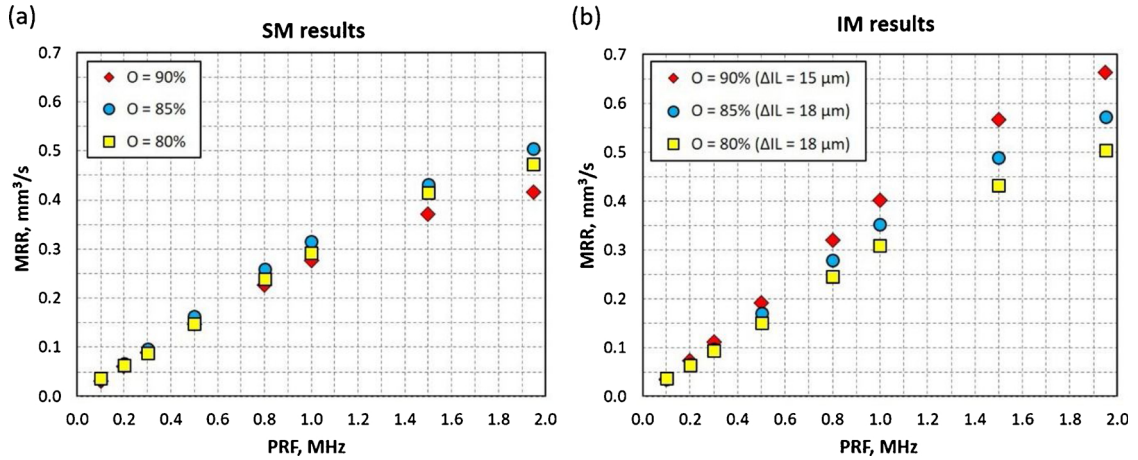

Fig. 12. Influence of PRF on MRR for: (a) SM and (b) IM using ΔIL = 15 µm for O = 90 % and ΔIL = 18 µm for O = 80 % and 85 %. The results were obtained using the Edgewave laser and F = 10.6 J/cm^2.

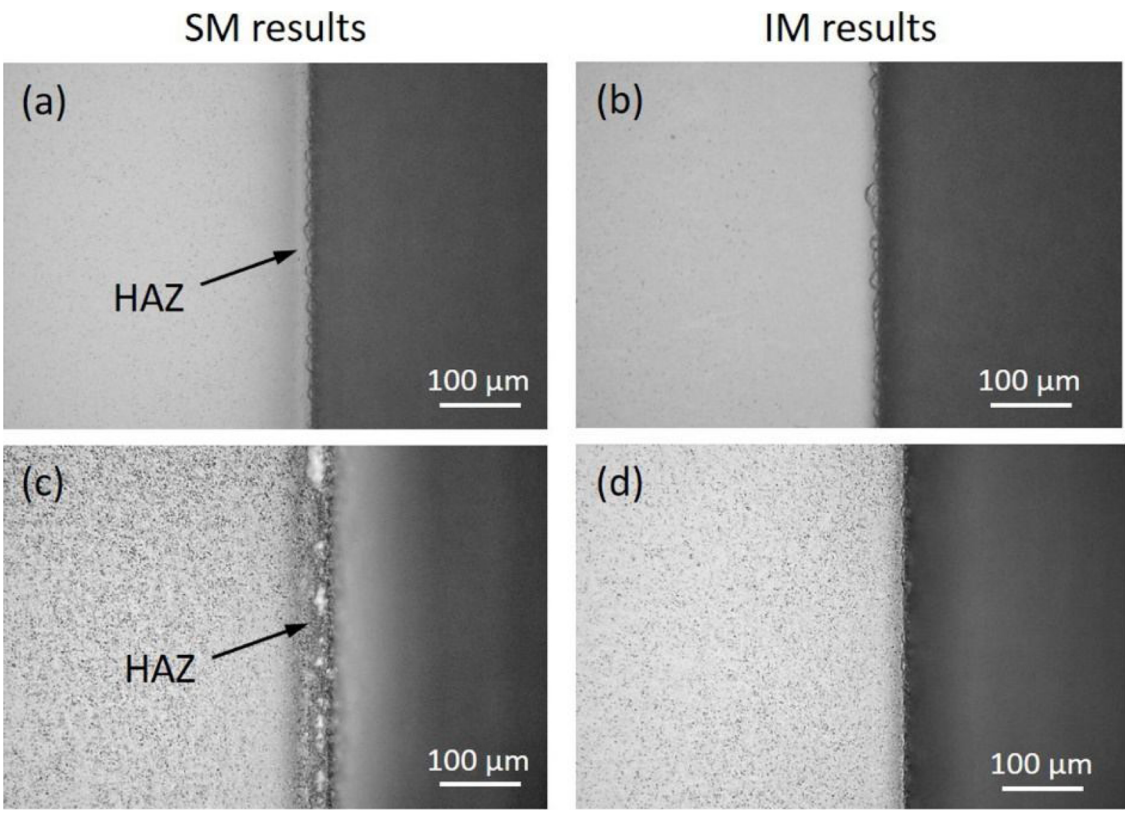

Fig. 13. Optical microscope image of the edges of the areas produced using the Edgewave laser and PRF = 200 kHz. The other machining parameters were as follows: (a) SM, F = 10.6 J/cm^2, O = 80 %, (b) IM with ΔIL = 18 µm, F = 10.6 J/cm^2, O = 80 %, (c) SM, F = 12.8 J/cm^2, O = 85 %, and (d) IM with ΔIL = 18 µm, F = 12.8 J/cm^2, O = 85 %.

MRR was also investigated using the Edgewave laser machining system. Detailed results are presented in the Supplementary Materials (see Figure S1 and S2). In general, it was observed that the machined depth as well as MRR increases almost in a linear manner with increasing laser fluence, whilst surface roughness of the areas generated using IM is significantly lower than those generated using SM (see Figure S2).

Finally, it was noted that external edges of the areas machined using SM were damaged by the laser-induced heat (see Fig. 13). For F = 12.8 J/cm^2, the heat-affected zone (HAZ) was relatively large and the glass surface was heavily contaminated. In the case of the areas produced by IM, the HAZ was very small and hardly seen using an optical microscope.

3.3. Recording the SM and IM processes using high-speed camera

The Phantom high-speed camera was used to record the SM and IM processes performed with the Trumpf laser machining system. This video can be found in the Supplementary Materials. During the video recording, the laser was machining two 1 mm × 0.5 mm areas. The first area was machined using SM, whereas the second was produced using IM with ΔIL = 18.3 µm. In both cases, the pulse overlap along the scan direction (O_S) was 95 %, whereas the hatch distance (ΔH) was 1.83 µm.

Fig. 14 shows eight snapshots from the SM process. The first three snapshots, see Fig. 14(a)–(c), show the moment when the laser beam starts machining the workpiece. Then the laser beam hits the smooth glass surface, removes the material and ejects small glass particles in the direction opposite to the laser beam scan direction, as indicated by the plume. In the next few scanning lines, see Fig. 14(d)–(f), the plume becomes weaker and it seems to be trapped inside the machined area. When the machined area gets wider, see Fig. 14(g) and (h), the plume changes direction because the laser beam is incident on a steep slope created by the material removed up to that point. This causes ejection of glass debris towards the already machined area. When the machining is performed using high laser fluence and high pulse overlap, the glass surface gets hot and some ejected glass particles fuse onto it.

In IM, as shown in Fig. 15, the glass material is removed layer by layer in each laser pass. Since the laser beam removes a relatively thin layer of glass, the incident angle of the laser beam is rather small and constant for each scan. Also the plume maintains its direction most of the time. The only exceptions are moments when the laser beam hits the boundaries of the machined area, as can be seen in Fig. 15(h). Finally, it should be noted that the machined area is significantly deeper and also cleaner than the one produced using SM.

4. Discussion

The results presented in Section 3 demonstrate that IM provides a higher removal rate of Borofloat®33 glass than conventional SM, thereby increasing the throughput of the ultrashort pulse laser micromachining process. This was particularly evident in the results obtained with the Trumpf picosecond laser system, where IM caused an MRR increase from 0.12 mm^3/s to even 0.53 mm^3/s. This was possible because IM provides: (i) more efficient ablation, i.e. higher machined depths for the same process parameters, e.g. comparing Figs. 9(a) and 4(c); (ii) more efficient machining using higher pulse overlaps and higher PRFs; and also (iii) more effective ejection of glass particles, as observed with the high-speed camera, thereby reducing the amount of glass particles firmly attached to the workpiece surface. With respect to surface roughness, IM often leads to higher Sq values, mainly because it produces periodic, parallel furrows. The periodicity of these furrows was found to correspond to the value of ΔIL. Fortunately, as demonstrated by (Wlodarczyk et al., 2019a), surface roughness can be reduced to S_q < 1 µm by applying a second laser pass in which a defocused laser beam is scanned in the direction orthogonal to the previous pass.

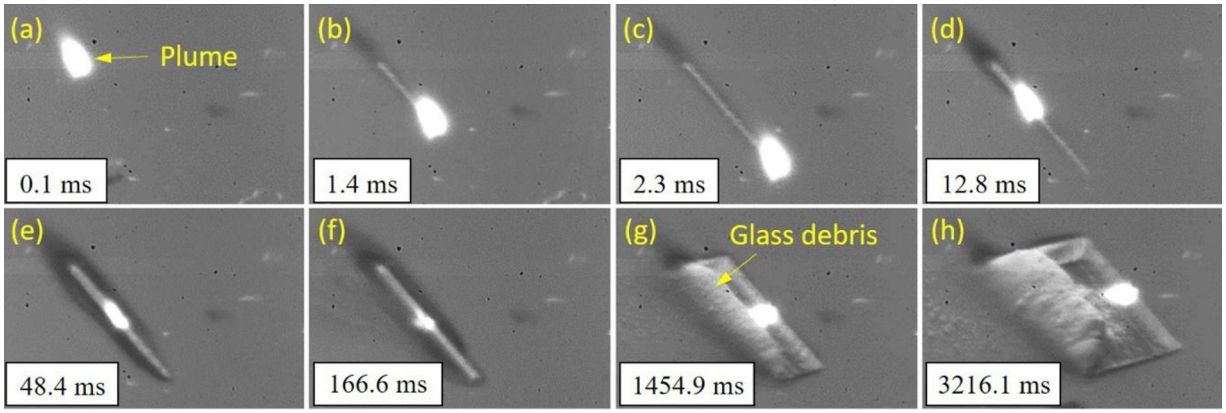

Fig. 14. Snapshots from the SM process recorded by the Phantom high-speed camera: (a)-(c) Beginning of machining (1st line), (d) 2nd line, (e) 5th line, (f) 15th line, (g) nth line, and (h) last line. Figures in the bottom left corner show the duration of the process.

Comparing the results presented in this article with the results published elsewhere (see Wlodarczyk et al., 2019b), where IM was used for the picosecond laser micromachining of Borofloat®33 glass using the second laser harmonic (λ = 515 nm), it can be concluded that this scanning method is more efficient and provides higher process throughput for the fundamental laser wavelength (λ = 1030 nm). For the shorter wavelength, the maximum MRR values were only 0.032 mm^3/s for SM (using O = 80 % and PRF = 100 kHz) and 0.075 mm^3/s for IM (using O = 95 % and PRF = 100 kHz). The machining improvement is therefore significantly smaller than that obtained using the fundamental laser wavelength. This is probably due to the fact that the machining at λ = 515 nm was performed using a smaller laser spot diameter (24 µm instead of 41 µm) and lower pulse energies (E_P < 65 µJ).

Although the presented results indicate that the machining of glass by using the 1030 nm wavelength leads to higher material removal rates, thereby increasing process throughput, it must be noted that at this wavelength the laser beam also caused damage to the rear surface of the glass, as shown in Fig. 3. This was due to the fact that the depth of field in this laser system was larger than the thickness of the workpiece. Therefore, to avoid these undesirable machining effects, thicker glass plates should be used. Fortunately in many applications, such as through-hole drilling or cutting, it often does not matter if the laser creates damage at the rear surface of the workpiece, providing that this damage is confined only to the machined area.

The damage to the rear surface of glass is initiated by the non-linear thermal lensing effect (also known as Kerr-lens focusing) that often occurs inside glass during ultrashort pulse laser machining. Because the material is transparent at a 1 µm wavelength and its surface is initially smooth, ultrashort laser pulses can penetrate into the material. Due to the thermal lensing effect, however, the laser beam becomes smaller while propagating in the material and this can initiate ablation of the rear glass surface when the intensity exceeds the ablation threshold value. When the laser beam ablates the rear glass surface, the material gets hotter and this increases its absorption and reduces the ablation threshold. The process at this stage is also enhanced by the incubation effect in which subsequent laser pulses reduce further the ablation threshold. This, in turn, maintains the ablation of the front surface of glass.

With the machining parameters provided by the Edgewave laser system the differences in MRR were not as pronounced as with the Trumpf picosecond laser; however analysis of the laser-machined surfaces (see Fig. 13) shows that IM still leads to “cleaner” machining and generates smaller HAZs. Since this laser system allows the machining of glass using very high PRF values, it was possible to obtain MRR as high as 0.65 mm^3/s. As shown in Fig. 12(b), the MRR value achieved with O = 90 % increases almost linearly with increasing PRF, and this suggests that for higher PRFs it should be possible to obtain even higher MRR values. Unfortunately, for PRF > 2 MHz this laser system produces pulses of reduced energy, thereby giving no improvement to process throughput. Also, it must be noted that the Edgewave laser system was capable of generating surfaces with relatively low roughness (S_q < 0.6 µm), as shown in Fig. 11(c). These results indicate that sub-picosecond laser pulses produced with a high repetition rate (PRF > 800 kHz) can provide significantly better machining results than the picosecond laser pulses.

Finally, the high-speed videos recorded by the Phantom camera show the mechanisms that lead to “cleaner” and more efficient

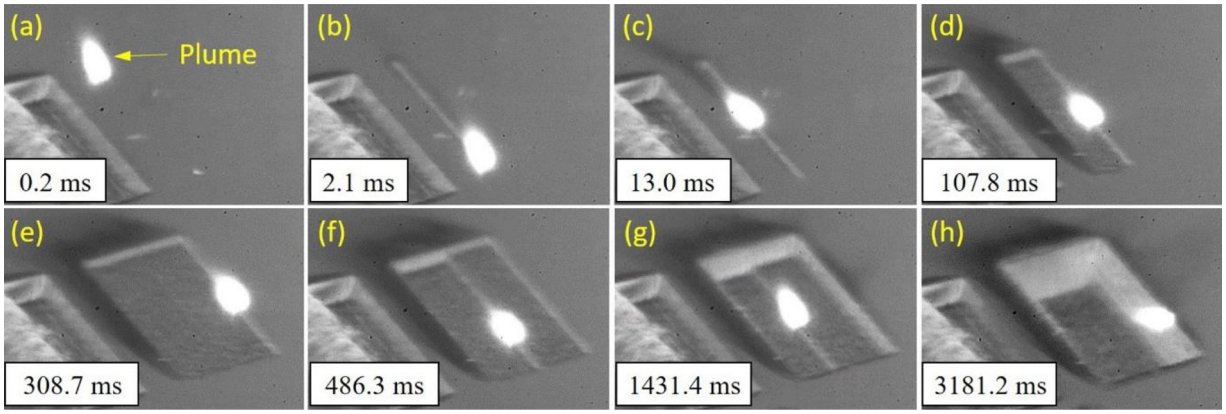

Fig. 15. Snapshots from the IM process recorded by the Phantom high-speed camera: (a) and (b) 1st line, (c) 2nd line, (d) 10th line, (e) last line in the 1st pass, (f) mth line in the 2nd pass, (g) nth line in the 5th pass, and (h) last line in the last pass. Figures in the bottom left corner show the duration of the process.

machining of glass with IM. In general, the removal of glass "layer-by-layer" causes the generation of "cleaner" and deeper areas, probably because the machined zone is less disrupted by glass particles generated during the laser process. The orientation of the plume in Fig. 15 suggests that glass particles are ejected in the direction opposite to the laser beam scan movement, landing away from the hot region. Since the machined layers are relatively shallow, the glass particles can easily escape the machined area even at low laser-induced recoil pressure. In the case of SM, after a few laser scans glass particles seem to travel towards the steep wall, as indicated by the plume in Fig. 14. Most of these glass particles bounce off and land very close to the laser beam scanning path. Since this area is very hot, they melt and merge with each other, forming a lump of partially fused white powder that sticks to the glass surface. Another reason why IM leads to more efficient machining can be a different incidence angle of the laser beam, which is normally smaller than that during SM. Since in SM the laser beam after a few scanning lines hits a steep wall, the actual laser fluence is decreased and hence is not as high as in IM, where for most of the time the laser beam machines a corrugated surface. A simplified model that illustrates this explanation can be found in (Wlodarczyk et al., 2019b).

5. Conclusions

This article demonstrates that a simple modification of the laser beam scanning strategy can lead to significant improvements of process throughput. By changing the scanning pattern from SM to IM, it was possible to increase the removal rate of glass from 0.12 mm^3/s to 0.53 mm^3/s with the Trumpf picosecond laser, using PRF = 400 kHz. In the case of SM, the machining could only be performed if PRF ≤ 100 kHz; higher values generated very rough surfaces which contained glass particles firmly attached to the glass surface. The machining of the same glass using the Edgewave sub-picosecond laser system provided similar results, i.e. the change of the scanning technique from SM to IM allowed MRR to increase from 0.50 to 0.65 mm^3/s. Such high removal rates were possible with PRF = 1.95 MHz. Using sub-picosecond laser pulses it was also possible to generate surfaces with relative low roughness (typically S_q < 0.8 µm when PRF > 400 kHz). To conclude, all these results show that IM provides many benefits over SM. Therefore, it is suggested that IM should become one of the standard hatch patterns available in commercial laser beam scanning programs. Finally, it should be highlighted that the benefits of using the IM method for laser machining of glass have been recently published as a patent application (Blair et al., 2019a, 2019b, 2019c).

CRediT authorship contribution statement

Krystian L. Wlodarczyk: Conceptualization, Methodology, Investigation, Visualization, Writing - original draft. **Joerg Schille:** Investigation, Writing - review & editing. **Lucas Naumann:** Investigation, Visualization. **Amiel A. Lopes:** Methodology, Investigation, Visualization. **Ioannis Bitharas:** Investigation, Visualization. **Prveen Bidare:** Investigation. **Stephen D. Dondieu:** Investigation. **Paul Blair:** Writing - review & editing. **Udo Loeschner:** Resources. **Andrew J. Moore:** Resources. **M. Mercedes Maroto-Valer:** Funding acquisition, Project administration, Supervision, Writing - review & editing. **Duncan P. Hand:** Resources, Supervision, Writing - review & editing.

Declaration of Competing Interest

The authors declare that they have no known competing financial interests or personal relationships that could have appeared to influence the work reported in this paper.

Acknowledgements

This research is part of the MILEPOST project (Grant agreement no.: 695070) funded by the European Research Council (ERC) under the European Union's Horizon 2020 Research and Innovation program. The received fund also covers the publication costs in open access. The paper reflects only the authors' view and ERC is not responsible for any use that may be made of the information it contains. The authors also thank the UK Engineering and Physical Sciences Research Council (Grant no.: EP/K030884/1) for providing access to the laboratory space and laser facilities, and Jolyon Cleaves from Vision Research for use of the Phantom V2512 high-speed camera.

Appendix A. Supplementary data

Supplementary material related to this article can be found, in the online version, at doi:https://doi.org/10.1016/j.jmatprotec.2020.116807.

References

Blair, P., Courtney, C., Parsonage, T., Lopes, A.A., Wlodarczyk, K.L., Hand, D.P., 2019a. Improvements in or relating to laser based machining. GB1721709.2A. .
Blair, P., Courtney, C., Parsonage, T., Lopes, A.A., Wlodarczyk, K.L., Hand, D.P., 2019b. Laser Based Machining of Glass Material. EP3511106A1. .
Blair, P., Courtney, C., Parsonage, T., Lopes, A.A., Wlodarczyk, K.L., Hand, D.P., 2019c. Laser Based Machining. US 2019/0193198A1. .
Bruening, S., Du, K., Jarczynski, M., Gillner, A., 2020. High-throughput micromachining with ultrashort pulsed lasers and multiple spots. J. Laser Appl. 32, 012003. https://doi.org/10.2351/1.5122853.
Exner, H., Hartwig, L., Ebert, R., Kloetzer, S., Streek, A., Schille, J., Loeschner, U., 2012. High speed laser micro processing using high brilliance continuous wave laser radiation. J. Laser Micro/Nanoengineering 7, 115–121. https://doi.org/10.2961/jlmn.2012.01.0023.
Gillner, A., Finger, J., Gretzki, P., Niessen, M., Bartels, T., Reininghaus, M., 2019. High power laser processing with ultrafast and multi-parallel beams. J. Laser Micro/Nanoengineering 14, 129–137. https://doi.org/10.2961/jlmn.2019.02.0003.
Hofmann, O., Stollenwerk, J., Loosen, P., 2020. Design of multibeam optics for high throughput parallel processing. J. Laser Appl. 32, 012005. https://doi.org/10.2351/1.5125778.
Loeschner, U., Schille, J., Streek, A., Knebel, T., Hartwig, L., Hillmann, R., Endisch, C., 2015. High-rate laser microprocessing using a polygon scanner system. J. Laser Appl. 27, S29303. https://doi.org/10.2351/1.4906473.
Malinowski, A., Gorman, P., Codemard, C.A., Ghiringhelli, F., Boyland, A.J., 2013. Pulsed fiber laser system with versatile pulse duration and shape. Opt. Lett. 38, 4686–4689.
Neuenschwander, B., Jaeggi, B., Zimmermann, M., Hennig, G., 2014. Influence of Particle Shielding and Heat Accumulation Effects Onto the Removal Rate for Laser Micromachining With Ultra-short Pulses at High Repetition Rates. ICALEO, pp. 218–226. https://doi.org/10.2351/1.5063063.
Neuenschwander, B., Jaeggi, B., Zimmermann, M., Markovic, V., Resan, B., Weingarten, K., de Loor, R., Penning, L., 2016. Laser surface structuring with 100 W of average power and sub-ps pulses. J. Laser Appl. 28, 022506. https://doi.org/10.2351/1.4944104.
Penning, L., Schluter, H., Hammers-Weber, P., 2016. Advanced scanning solutions for micromachining. Laser User 30–32.
Saraceno, C.J., Sutter, D., Metzger, T., Abdou Ahmed, M., 2019. The amazing progress of high-power ultrafast thin-disk lasers. J. Eur. Opt. Soc. Publ. 15, 15. https://doi.org/10.1186/s41476-019-0108-1.
Schille, J., Schneider, L., Loeschner, U., 2015. Process optimization in high-average-power ultrashort pulse laser microfabrication: how laser process parameters influence efficiency, throughput and quality. Appl. Phys. A-Mater. 120, 847–855. https://doi.org/10.1007/s00339-015-9352-4.
Schille, J., Schneider, L., Streek, A., Kloetzer, S., Loeschner, U., 2016. High-throughput machining using a high-average power ultrashort pulse laser and high-speed polygon scanner. Opt. Eng. 55, 096109.
Wlodarczyk, K.L., Kaakkunen, J.J.J., Vahimaa, P., Hand, D.P., 2014. Efficient speckle-free laser marking using a spatial light modulator. Appl. Phys. A-Mater. 116, 111–118. https://doi.org/10.1007/s00339-013-8186-1.
Wlodarczyk, K.L., Hand, D.P., Maroto-Valer, M.M., 2019a. Maskless, rapid manufacturing of glass microfluidic devices using a picosecond pulsed laser. Sci. Rep. 9, 20215. https://doi.org/10.1038/s41598-019-56711-5.
Wlodarczyk, K.L., Lopes, A.A., Blair, P., Maroto-Valer, M.M., Hand, D.P., 2019b. Interlaced laser beam scanning: a method enabling an increase in the throughput of ultrafast laser machining of borosilicate glass. J. Manuf. Mater. Process. 3, 1–15. https://doi.org/10.3390/jmmp3010014.